Chapter 21
Parameter Estimation via Instantaneous Frequency and Damping from Transient Ring-Down Data

Robert J. Kuether and Matthew R.W. Brake

Broadband impact excitation in structural dynamics is a common technique used to detect and characterize nonlinearities in mechanical systems since it excites many frequencies of a structure at once. Nonstationary time signals from transient ring-down measurements require time-frequency analysis tools to observe variations in frequency and energy dissipation as the response evolves. This chapter uses the Short-Time Fourier Transform (STFT) to estimate the instantaneous parameters from measured or simulated data. By combining the discrete Fourier transform with an expanding or contracting window function that moves along the time axis, the resulting spectra are used to estimate the instantaneous frequencies, damping ratios, and complex Fourier coefficients. Other methods such as Hilbert transforms in conjunction with the Zeroed Early Fast Fourier Transform (ZEFFT) (Allen and Mayes 2010) or wavelet based approaches (Kerschen et al. 2006) are also able to be applied in similar manners as the STFT. From any of these methods, the amplitude-frequency dependence in the damped response is able to be extracted in order to determine the parameters for a joint model.

21.1 Overview of Spectra Calculation Methods

Analyzing vibration responses in the frequency domain has long provided insight into the dynamics of linear structures, such as the identification of invariant modal frequencies and damping ratios from transient ring-down data. The most

R.J. Kuether
Sandia National Laboratories, Albuquerque, NM, USA

M.R.W. Brake (✉)
William Marsh Rice University, Houston, TX, USA
e-mail: brake@rice.edu

M.R.W. Brake (ed.), *The Mechanics of Jointed Structures*,
DOI 10.1007/978-3-319-56818-8_21

widespread tool for frequency-domain analysis is the Fourier transform, partly due to the efficiency of the Fast Fourier Transform (FFT) algorithm (Cooley and Tukey 1965). One of the limitations of this method is that it only provides meaningful information for linear systems and responses that are stationary and periodic (albeit windowing a time signal lightens the latter requirement). Nonlinear systems and nonstationary time signals require a new set of tools for frequency-domain analysis of transient responses. One example is the zero-crossing detection method, developed in Londoño et al. (2015), which uses the zero-crossings of the time signal to estimate the instantaneous frequency and decaying envelope of a nonlinear system. The review of Neild et al. (2003) provides a thorough discussion of various time-frequency distribution tools such as moving window discrete Fourier transform, moving window auto-regressive model, and harmonic wavelet transform. These signal processing tools can be used to identify how the instantaneous frequency and damping of a measurement changes as a function of time, or response amplitude, providing system parameters conceptually similar to those obtained from linear systems. A number of techniques have been developed to estimate the time-varying frequency and damping from transient ring-down data, as discussed in what follows.

21.1.1 The Hilbert Transform

The Hilbert transform is defined as the convolution of a time history $x(t)$ and the function $1/(\pi t)$

$$H(x(t)) = \int_{-\infty}^{\infty} x(\tau) \frac{1}{\pi(t-\tau)} \mathrm{d}\tau. \tag{21.1}$$

This transformation calculates the analytic representation of the measurement $x(t)$, from which the amplitude dependent properties of a system can be extracted. Feldman developed the 'FREEVIB' method in Feldman (1994) by processing the free vibration response with the Hilbert transform and determining a single-degree-of-freedom (SDOF) modal model based on the analytic signal and its time derivatives. Later Sumali and Kellogg (2011) improved on this method by fitting the analytic signal to a polynomial function in order to better estimate the phase and decaying envelope. The curve fitting procedure is developed to smooth the effects of noise during experimentation (Sumali and Kellogg 2011; Sracic et al. 2012; Deaner et al. 2015).

The Hilbert transform is somewhat limited when applied with broadband excitation because this method assumes that the response behaves as a monophase, SDOF oscillator. These approaches require additional data processing (e.g., band-pass filtering) for signals with multiple harmonic components. One approach to process nonstationary signals with multiple harmonics uses empirical mode decomposition (EMD) to create a set of intrinsic mode functions that are then processed using a Hilbert transformation (Huang et al. 1998).

21.1.2 Wavelet Transformations

Wavelet transformations generally condition the time history $x(t)$ by multiplying it by a series of square integrable functions (termed wavelets) that effectively window the data over a narrow range (in this case, in time). In this manner, the response of the system for a given amplitude is able to be analyzed in isolation, without contamination from higher or lower amplitude excitations that occurred earlier or later in the time history, respectively. As compared to the original STFT, the wavelet transformation is developed to specifically account for adequately resolving both high and low frequency responses by using windowing functions such as the Morlet wavelet (Goupillaud et al. 1984/85; Lin and Qu 2000).

A nonlinear system identification and model reduction strategy using EMD, wavelet transforms, and slow flow constructions is presented in Chap. 20, with further details given in Eriten et al. (2013), Lee et al. (2009), and Vakakis et al. (2011). In Kurt et al. (2015), the method is further developed for a model updating strategy for mechanical systems with local nonlinearities by comparing the instantaneous frequencies and energies from simulated broadband excitation using the wavelet transform. The "empirical" instantaneous frequencies and amplitudes are compared with the undamped nonlinear normal modes (NNMs) (Kerschen et al. 2009; Vakakis 1997) of the underlying Hamiltonian system as a metric to update the model.

21.1.3 The Short-Time Fourier Transform

In this chapter, the STFT is used to estimate the instantaneous frequencies and damping ratios from measurements under broadband excitation. The STFT takes a discrete Fourier transform of small windowed sections of the response to estimate the frequency content at a given time-point (similar to a wavelet transformation). In this work, the frequency-domain tool is modified to allow the short-time period of the window function to expand or contract as it slides down the time axis, allowing for better averaging of the frequencies and amplitudes. This approach is essentially that of the wavelet transform. From the processed time-frequency distribution, a peak picking method identifies the instantaneous "natural frequency" and complex amplitude of the Fourier coefficient from which the instantaneous damping ratio is estimated. These amplitude dependent properties of the system have a wide range of applications including nonlinear detection, characterization, and potentially quantification.

The chapter is outlined as follows: Sect. 21.2 presents the theoretical developments of the modified STFT algorithm along with the approach to extract the instantaneous frequency and damping as a function of response amplitude. In order to demonstrate this methodology, Sect. 21.3 processes measured time data from

two beams assembled with a lap joint (i.e., the Brake–Reuß beam) and estimates the parameters of an Iwan model from the instantaneous frequencies and damping ratios.

21.2 Theoretical Development of the Parameter Estimation Technique

The STFT operates on the freely decaying time signal $x(t)$ of a nonlinear mechanical system measured over a period T. The signal is sampled at N evenly spaced points in time such that the increment is defined as $\Delta = T/N$, resulting in N discrete measurements $x_0, x_1, \ldots, x_{N-1}$ with $x_n = x(n\Delta)$. A window function $w(t-\tau)$ moves along the time axis at discrete time shifts $\tau = m\Delta$ and has a much shorter time period than the measurement period (i.e., $T_w \ll T$). The discretized window is sampled at the same N points in time, denoted as $w_{0-m}, w_{1-m}, \ldots, w_{N-1-m}$ where $w_{n-m} = w((n-m)\Delta)$ and is applied to the signal prior to taking the Fourier transform. The time point m controls the center time of the window, allowing a Fourier transform to be taken from different sections of the signal and the instantaneous frequency content to be approximated. Mathematically, the discrete Fourier transform of the windowed signal is taken as

$$X(k,m) = \sum_{n=0}^{N-1} x_n w_{n-m} e^{-\mathrm{i}2\pi kn/N} \tag{21.2}$$

defined at discrete frequencies

$$\omega_k = \frac{2\pi k}{T}. \tag{21.3}$$

One of the challenges with using the STFT is that the period of the window function T_w dictates the accuracy and resolution of the spectrum. For example, if the window period is too large, then the frequency of the signal will be poorly averaged. Conversely, if the window is too small, then the poor frequency resolution makes it difficult to approximate the instantaneous frequency. In an effort to improve this, the STFT is modified to allow for the time period of the window to change as it moves down the time axis, making the period $T_w(m)$ explicitly dependent on the time instant m. This ability to either expand or contract the window size helps produce an STFT with better averaging and resolution. The modified STFT becomes

$$X(k,m) = \sum_{n=0}^{N-1} x_n w_{n-m}(m) e^{-\mathrm{i}2\pi kn/N} \tag{21.4}$$

and from this, the approximation of the Fourier series coefficients is

$$\hat{X}(k,m) = \frac{2X(k,m)}{\sum_{n=0}^{N-1} w_{n-m}(m)}. \tag{21.5}$$

Each windowed Fourier transform is related to the time point at the center of the window

$$t_{cw}(m) = \frac{mT}{N} + \frac{T_w(m)}{2}. \tag{21.6}$$

Unlike the discrete Fourier transform, the STFT is a two-dimensional spectrum that changes as the window moves on the time axis. The moving window is zero-padded to improve the frequency resolution, but this does not actually improve on the estimation of the Fourier coefficients in Eq. (21.5). A variety of window functions can be used (e.g., Rectangle, Hamming, etc.) depending on the application of interest. The Hanning window generally offers good results for transient ring-down data and is thus the one used throughout this work. The discretized function for the time-varying Hanning window is

$$w_{n-m}(m) = \begin{cases} \frac{1}{2}\left(1 - \cos\left(\frac{2\pi(n-m)T}{T_w(m)N}\right)\right) & 0 \le (n-m)\frac{t}{N} < T_w(m) \\ 0 & \text{otherwise.} \end{cases} \tag{21.7}$$

The period of the Hanning window explicitly depends on the time instant m allowing for the period to expand or contract as the window moves position. In what follows, only three forms for $w(m)$ are considered: a constant window, a linearly varying window, and an exponentially varying window. The constant window is the original definition of the STFT. The linear and exponentially varying windows are more appropriate for signals that decrease in frequency as time increases (and energy decreases in the ring-down data). The variable window gives more flexibility when analyzing nonstationary signals and results in a better estimate of the instantaneous frequency content.

21.2.1 Instantaneous Stiffness and Damping Estimation from Ring-Down Data

The transient ring-down response $x(t)$ can be represented as a summation of decaying harmonic functions of the form

$$x(t) = \sum_{r=1}^{P} \mathrm{Re}\{A_{r,0} e^{-\beta_r(t)t} e^{\mathrm{i}\phi_r(t)}\}. \tag{21.8}$$

The assumed form of the signal has a total of p decaying harmonic functions each having an initial complex amplitude $A_{r,0}$, time dependent decay rate $\beta_r(t)$, and time dependent phase $\phi_r(t)$. Time-frequency analyses such as the modified STFT described above are needed to identify the time dependency of the phase and decay rate. Following the approach in Sumali and Kellogg (2011), the decay rate and phase are rewritten as

$$\beta_r(t) = \zeta_r(t)\omega_r(t) \tag{21.9}$$

$$\phi_r(t) = \omega_{r,D}(t)t. \tag{21.10}$$

In keeping notation with the free response of an underdamped, linear oscillator, the decaying harmonic functions are described by a time dependent damping ratio $\zeta_r(t)$, and damped and undamped natural frequencies $\omega_{r,D}(t)$ and $\omega_r(t)$, respectively. Substituting Eqs. (21.9) and (21.10) into Eq. (21.8) would produce a form similar to the linear solution. The time dependent frequencies and damping ratios are estimated from the STFT data by using peak picking methods. The damped frequency occurs where there is a maximum absolute value of the Fourier coefficient, within a specified frequency range of the spectrum for each windowed response.

Thus, the goal is to define a method to calculate $\omega_r(t)$, $\zeta_r(t)$, and $A_{r,0}$ for the rth decaying harmonic function in Eq. (21.8). The same process is repeated to extract the coefficients of other harmonic functions from the same STFT data by looking for peaks in a different frequency range. Starting with the collection of Fourier coefficients in Eq. (21.5) with a center time $t_{cw}(m_j)$, the maximum amplitude of $\hat{X}(k, m_j)$ is found within a subset of frequencies defined by the set $\{k_l \quad k_u\}$, as given by Eq. (21.3). The maximum amplitude of the Fourier coefficient is determined via

$$A_r(t_{cw}(m_j)) = \max_{k\in\{k_l,\, k_u\}} \left(\left| \hat{X}(k, m_j) \right| \right), \tag{21.11}$$

and the damped frequency at the peak is

$$\omega_{r,D}(t_{cw}(m_j)) = \frac{2\pi k_{\max}}{T}. \tag{21.12}$$

Taking the magnitude of the rth decaying harmonic function, this is related to the peak Fourier coefficient at window time $t_{cw}(m_j)$ as

$$A_r(t_{cw}(m_j)) = |A_{r,0}| e^{-\beta_r(t_{cw}(m_j))t_{cw}(m_j)}. \tag{21.13}$$

This equation alone does not uniquely solve for all unknown values of $A_{r,0}$ and $\beta_r(t_{cw}(m_j))$, so it is assumed that the decay rate at the end of the windowed response has decayed to a linear response amplitude such that

$$\beta_r(t_{cw}(m_{\text{end}-1})) = \beta_r(t_{cw}(m_{\text{end}})). \tag{21.14}$$

Combining this relationship with Eq. (21.13) offers the unique solution to $A_{r,0}$ and $\beta_r(t_{cw}(m_j))$.

Assuming that the damped natural frequency relates to the undamped frequency via

$$\omega_{r,D}(t_{cw}(m_j)) = \omega_r(t_{cw}(m_j))\sqrt{1-\zeta_r^2(t_{cw}(m_j))}, \tag{21.15}$$

the instantaneous (undamped) frequency is estimated by combining Eqs. (21.9) and (21.15)

$$\omega_r(t_{cw}(m_j)) = \sqrt{\omega_{r,D}^2(t_{cw}(m_j)) + \beta_r^2(t_{cw}(m_j))}. \tag{21.16}$$

Thus, the instantaneous damping ratio is defined to be

$$\zeta_r(t_{cw}(m_j)) = \frac{\beta_r(t_{cw}(m_j))}{\omega_r(t_{cw}(m_j))}. \tag{21.17}$$

21.3 Application to the Brake–Reuß Beam

To demonstrate the application of the STFT method for determining joint parameters, measurements from the Brake–Reuß beam (Chap. 9) are used. For this example, the Brake–Reuß beam is suspended via bungee cords, and an impact hammer is used to provide a broadband excitation to the system. The impact force from the hammer is recorded by its load cell and records of acceleration time histories are obtained from accelerometers mounted on the beam. The bolts are torqued to 15 Nm for the data reported here, and the experimental setup for these tests is shown in Fig. 21.1.

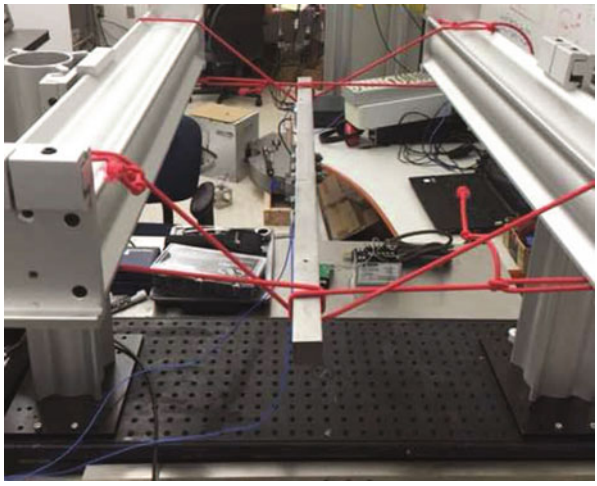

Fig. 21.1 Experimental setup for the impact hammer tests on the Brake–Reuß beam

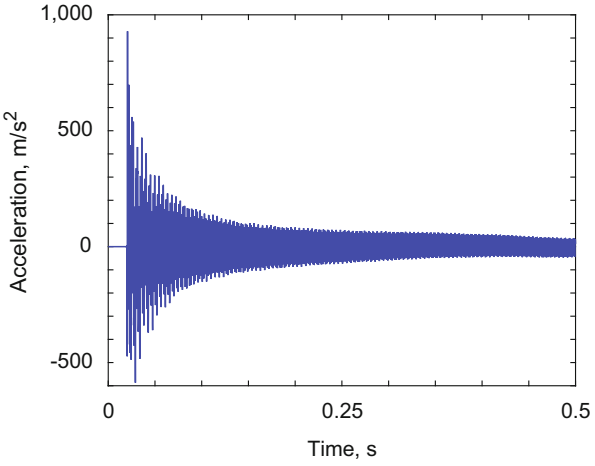

Fig. 21.2 Representative time history for a large amplitude impulse excitation

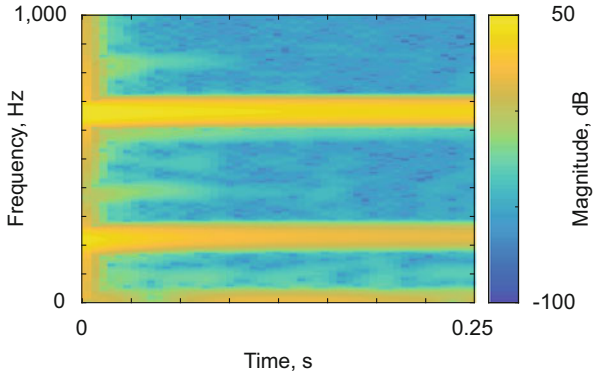

Fig. 21.3 Spectrogram for the time history shown in Fig. 21.2

A typical response for a large amplitude impact is shown in Fig. 21.2. Due to the lap joint located in the center of the system, the response is dependent upon excitation amplitude. That is, as the response amplitude decreases, the system is expected to stiffen (increase in frequency) due to a transition from macroslip to microslip, and the amount of energy dissipated per oscillation is expected to reduce (again, due to the transition from macroslip to microslip). In these specific experiments, the system is not excited to macroslip since that would plastically damage the system. Consequently, the shift from high amplitudes to low amplitudes is subtle, but still observable in Fig. 21.3, which is the spectrogram of the time history response from Fig. 21.2.

In order to deduce the parameters to describe the interface with a RIPP joint (Chap. 16), 18 different impact tests are used in which the impact excitation is varied

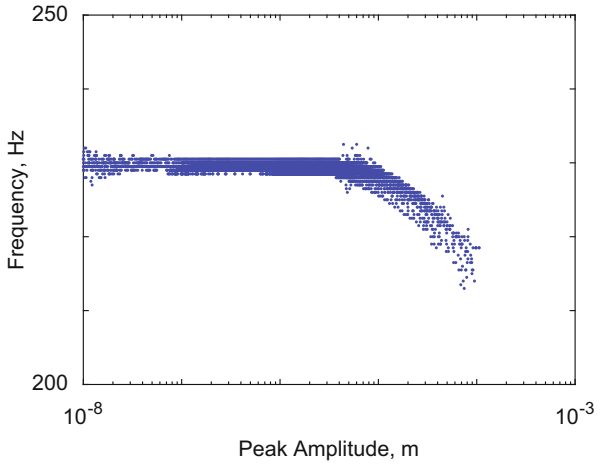

Fig. 21.4 Frequency versus amplitude data synthesized from 18 different impact tests

from approximately 100 to 2000 N. While 18 tests are used, only a subset is needed to deduce a set of parameters for a RIPP joint model; the benefit of 18 tests is in being able to develop a statistical distribution of parameters for the RIPP joint model that describe test-to-test variability. The development of a statistical distribution of parameters is further discussed in Bonney et al. (2016); here, the derivation of each parameter is discussed in detail as an example of parameter estimation techniques for the RIPP joint model. One important caveat is that in systems with multiple modes in the response, such as the present system, the following techniques are for deriving the modal joint properties [see, for instance, Deaner et al. (2015), Roettgen et al. (2014)] instead of global joint properties; however, for the purpose of this example, the properties are derived as if the response is unimodal by first applying a modal filter to the data.

The stiffness of the system is inferred from the evolution of the primary natural frequency with response amplitude (Fig. 21.4). For response amplitudes below 4 μm, the natural frequency is constant at approximately 230 Hz. Some noise is observed, though, due to the process of extracting frequency and dissipation data from the impact experiments. At response amplitudes above 4 μm, a significant decrease is observed in the natural frequency such that at an amplitude of 100 μm, the natural frequency is approximately 213 Hz. This change in frequency ($\triangle\omega$) is directly related to K_T as

$$K_T = M \times \triangle\omega^2 \approx 1.1 \times 10^6 \,\mathrm{N/m}. \tag{21.18}$$

In this calculation (with the unimodal assumption), M is taken as the system mass, 3.67 kg.

A second quantity that can be discerned from the stiffness plot is ϕ_{MAX}, which is later used to deduce F_S. Here, as macroslip is not observed in the data, ϕ_{MAX}

is approximated as ten times the largest response amplitude since the system does not transition to complete macroslip. In this case, $\phi_{MAX} = 2\,\text{mm}$. The consequence of this approximation is that this parameter is valid for the experiments reported, but "small" errors are expected to occur for larger excitation amplitudes as no data regarding macroslip is recorded. The term "small" is used as the model is still expected to be reasonable, but not precise in describing the transition from microslip to macroslip.

The STFT method also calculates the damping ratio as a function of excitation amplitude. Using the definition of the log decrement

$$\delta = \frac{2\pi\zeta}{\sqrt{1-\zeta^2}} = \log\left(\frac{x_j}{x_{j+1}}\right), \tag{21.19}$$

with two adjacent peaks in a decaying transient signal having amplitudes x_j and x_{j+1}, the dissipation per cycle $\mathscr{D}$ is calculated as the difference in energy between the two peaks

$$\mathscr{D} = \frac{1}{2}\omega^2 M A_0^2\left(\left(e^{2\pi\zeta/\sqrt{1-\zeta^2}}\right)^2 - 1\right), \tag{21.20}$$

where A_0 is the response amplitude. From Segalman (2005), $\mathscr{D}$ is directly related to χ by the slope of $\mathscr{D}$ as a function of amplitude on a log–log plot being $3 + \chi$. From the dissipation information in Fig. 21.5, $\chi \approx -0.76$. The features of the plot near the start of each set of data (i.e., at high amplitudes where the dissipation curves have negative slopes) are artifacts of the signal processing techniques.

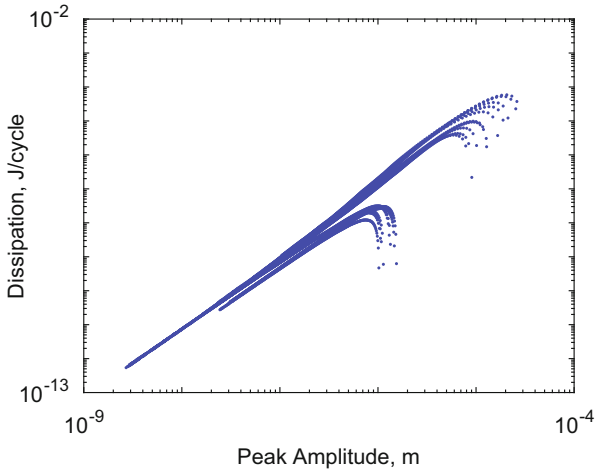

Fig. 21.5 Calculated energy dissipation curves from 18 different impact tests

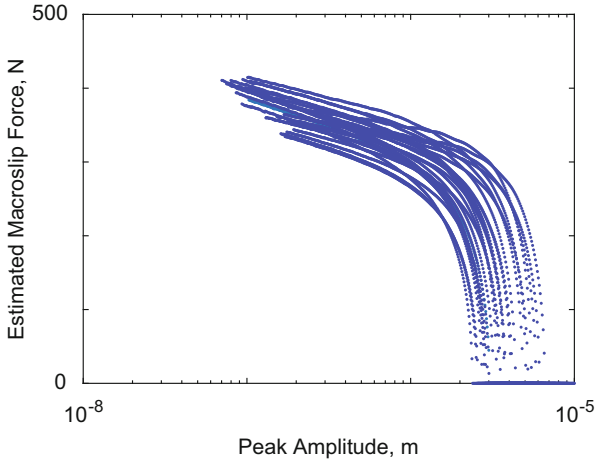

Fig. 21.6 Calculated macroslip force value from low amplitude impact tests

To calculate the remaining two parameters, β and F_S, first F_S is estimated from ϕ_{MAX} as

$$F_S \approx \phi_{MAX} M \omega_\phi^2, \tag{21.21}$$

with frequency ω_ϕ at the response amplitude equal to ϕ_{MAX} (or largest recorded amplitude when macroslip is not observed). Second, β is calculated using this approximation via (Segalman 2005)

$$\beta = \left(\frac{F_S}{\phi_{MAX} K_T} - \frac{\chi + 1}{\chi + 2} \right) \Bigg/ \left(1 - \frac{F_S}{\phi_{MAX} K_T} \right). \tag{21.22}$$

As macroslip is not observed in the experiments, these results are valid only for low response amplitudes as the constitutive behavior of the joint at low amplitudes is dominated by the tangential stiffness K_T shown in Fig. 21.6. Each of the parameters deduced from the experiments reported in Bonney et al. (2016) is summarized in Table 21.1.

21.4 Perspectives on the Short-Time Fourier Transform Method

In this chapter, a modification to the STFT is presented and used to extract the instantaneous frequency and damping ratio from measured transient ring-down responses. The short-time period of the window function can expand or contract

Table 21.1 Joint parameters deduced from the experiments of Bonney et al. (2016)

Property	Value
Tangential stiffness, K_T	1.1×10^6 N/m
Macroslip displacement, ϕ_{MAX}	2 mm
Macroslip force, F_S	400 N
Dissipation exponent, χ	-0.76
Stiffness ratio, β	0.16
Pinning stiffness, K_P	10^7 N/m
Pinning clearance, δ_P	2 mm

as it moves down the time axis, allowing for better estimates of the frequency content at a given time instant. The time-frequency distribution is then used to find the peak Fourier coefficients in the spectra and estimate the instantaneous natural frequency and damping ratio. One advantage to this approach is that it can be applied to any time signal with multi-harmonic components without the need to do any preprocessing such as band-pass or modal filtering.

The methodology is demonstrated on experimental measurements taken from the Brake–Reuß beam. The response spectra show how nonlinearities in jointed structures can be detected for various amplitudes of excitation. The lap joint has a softening effect on the overall stiffness and introduces amplitude dependent damping that increases with response amplitude.

References

M.S. Allen, R.L. Mayes, Estimating degree of nonlinearity in transient responses with zeroed early-time fast Fourier transforms. Mech. Syst. Signal Process. **24**, 2049–2064 (2010)

M.S. Bonney et al., Experimental determination of frictional interface models, in *34th International Modal Analysis Conference (IMAC XXXIV)*, Orlando, FL, 2016

J.W. Cooley, J.W. Tukey, An algorithm for the machine calculation of complex Fourier series. Math. Comput. **19**, 297–301 (1965)

B.J. Deaner et al., Application of viscous and Iwan modal damping models to experimental measurements from bolted structures. ASME J. Vib. Acoust. **137**, 021012 (2015)

M. Eriten et al., Nonlinear system identification of frictional effects in a beam with a bolted joint connection. Mech. Syst. Signal Process. **39**, 245–264 (2013)

M. Feldman, Non-linear system vibration analysis using Hilbert transform - I. Free vibration analysis method "Freevib". Mech. Syst. Signal Process. **8**, 119–127 (1994)

P. Goupillaud, A. Grossmann, J. Morlet, Cycle-octave and related transforms in seismic signal analysis. Feoexploration **23**, 85–102 (1984/1985)

N.E. Huang et al., The empirical mode decomposition and the Hilbert spectrum for nonlinear and non-stationary time series analysis. Proc. R. Soc. Lond. A: Math. Phys. Eng. Sci. **454**, 903–995 (1998)

G. Kerschen et al., Past, present and future of nonlinear system identification in structural dynamics. Mech. Syst. Signal Process. **20**, 505–592 (2006)

G. Kerschen et al., Nonlinear normal modes. Part I. A useful framework for the structural dynamicist. Mech. Syst. Signal Process. **23**, 170–194 (2009)

M. Kurt et al., Methodology for model updating of mechanical components with local nonlinearities. J. Sound Vib. **357**, 331–348 (2015)
Y.S. Lee et al., Physics-based foundation for empirical mode decomposition: correspondence between intrinsic mode functions and slow flows. AIAA J. **47**, 938–2963 (2009)
J. Lin, L. Qu, Feature extraction based on Morlet wavelet and its application for mechanical fault diagnosis. J. Sound Vib. **234**, 135–148 (2000)
J.M. Londoño, S.A. Neild, J.E. Cooper, Identification of backbone curves of nonlinear systems from resonance decay responses. J. Sound Vib. **348**, 224–238 (2015)
S.A. Neild, P.D. McFadden, M.S. Williams, A review of time-frequency methods for structural vibration analysis. Eng. Struct. **25**, 713–728 (2003)
D.R. Roettgen et al., Feasibility of describing joint nonlinearity in exhaust components with modal Iwan models, in *ASME International Design Engineering Technical Conferences IDETC/CIE*, Buffalo, NY, 2014
D.J. Segalman, A four-parameter Iwan model for lap-type joints. ASME J. Appl. Mech. **72**, 752–760 (2005)
M.W. Sracic, M.S. Allen, H. Sumali, Identifying the modal properties of nonlinear structures using measured free response time histories from a scanning laser Doppler vibrometer, in *30th International Modal Analysis Conference (IMAC XXX)*, Jacksonville, FL, 2012
H. Sumali, R.A. Kellogg, Calculating damping from ring-down using Hilbert transform and curve fitting, in *4th International Operational Modal Analysis Conference*, Istanbul, 2011
A.F. Vakakis, Nonlinear normal modes (NNMs) and their applications in vibration theory: an overview. Mech. Syst. Signal Process. **11**, 3–22 (1997)
A.F. Vakakis et al., Current efforts towards a non-linear system identification methodology of broad applicability. Proc. Inst. Mech. Eng. Part C: J. Mech. Eng. Sci. **225**, 2497–2515 (2011)